Modelling of HREM and nanodiffraction for dislocation kinks and core reconstruction

2000 J. Phys.: Condens. Matter 12 10175

(http://iopscience.iop.org/0953-8984/12/49/317)

J. Phys.: Condens. Matter **12** (2000) 10175–10183. Printed in the UK PII: S0953-8984(00)17508-3

Modelling of HREM and nanodiffraction for dislocation kinks and core reconstruction

C Koch†, J C H Spence†, C Zorman‡, M Mehregany‡ and J Chung§

† Department of Physics and Astronomy, Arizona State University, Tempe, AZ 85287, USA
‡ Department of Electrical Engineering and Computer Science, Case Western Reserve University, Cleveland, OH 44106, USA
§ Department of Materials Science and Engineering, Case Western Reserve University, Cleveland, OH 44106, USA

Received 28 September 2000

Abstract. The ability to directly image individual dislocation kinks (Kolar H *et al* 1996 *Phys. Rev. Lett.* **77** 4031) opens up many possibilities for the study of kink dynamics by *in situ* TEM. Unfortunately, this technique is limited by surface roughness. For ceramics, however, high temperature annealing has been found to produce inert and atomically smooth surfaces that even survive ambient pressures (Susnitzky D 1992 *J. Am. Ceram. Soc.* **75** 2463). We have prepared such samples of 3C-SiC, in order to image kinks by the forbidden reflections method. Using multislice simulations for 30 and 90° partial dislocations in Si we show that not only the number of kinks along the dislocation core can be determined, but also their structure assuming an aberration corrected TEM.

We also show how the recently proposed double period reconstruction along the 90° partial dislocation in Si can easily be verified experimentally using convergent beam electron diffraction.

1. Introduction

Experimental evidence for the reconstruction and periodicity of dislocation cores in semiconductors is largely indirect, consisting mainly of the results of relaxed total energy calculations [1, 6, 7] and estimates of the number of unpaired spins along cores, as measured by EPR (for a review, see [2]). On this basis, a consensus has developed that reconstruction clears the gap of deep states for both the 30 and 90° partials in Si. For most other systems, the situation is less clear, and an experimental method for direct measurement of core periods would be valuable. Similarly, the direct observation of dislocation kinks has recently become possible [3] using forbidden reflection lattice imaging (FRLI), in which the dislocation is viewed from the side using kinematically 'forbidden' reflections [15]. This method can give estimates of kink density (and hence the kink formation energy F_K), but is limited by the effects of surface roughness on an atomic scale. It is known, however, that for many refractory crystals, an atomically smooth surface can be achieved under modest vacuum conditions after a high temperature anneal [4]. In this paper we propose a new nanodiffraction method for measuring core periods, and consider whether, using the latest one ångström resolution HREM machines, the FRLI method can distinguish dislocation kink models.

0953-8984/00/4910175+09$30.00

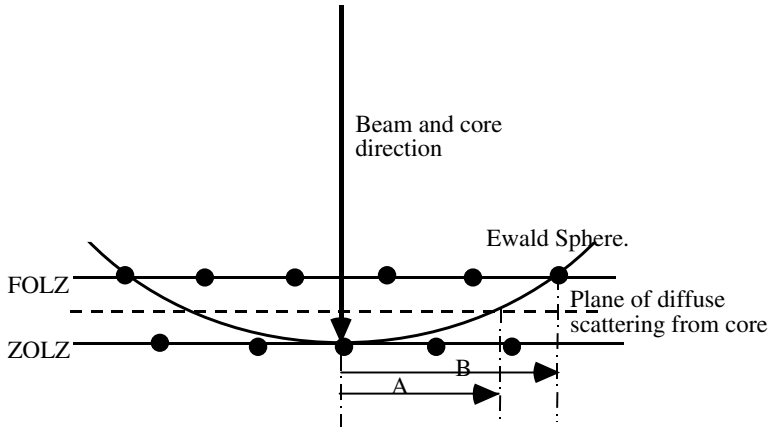

Figure 1. Ewald sphere geometry for observing dislocation core period doubling by CBED. A doubling of atomic periodicity would produce the dashed plane of diffuse scattering shown, which intersects the Ewald sphere on a circle. The ratio of the distances A/B is $1/\sqrt{2}$ for high energies.

2. Image and CBED simulations

In order to better interpret experimental partial dislocation kink images [3] and find ways to increase their quality, we performed a number of multislice calculations. Such calculations were also done to give our proposed method for detecting the periodicity of the 90° partial dislocation reconstruction using convergent beam electron diffraction (CBED) a more quantitative basis. We used the program 'mulslice' [5], which we modified to allow us to make the slice thickness as thin as 0.5 Å assigning the potential of the atoms to more than a single slice. Temperature effects were accounted for by a Debye–Waller factor of 0.44 $Å^2$ for Si. All multislice calculations were done using 1024×1024 beams.

The atomic coordinates for the different core reconstruction and kink models were taken from tight-binding total-energy calculations performed by Nunes *et al* [6]. We designed two models for the HREM simulations, one with a 30° and the other one with a 90° partial dislocation. In order to make the simulations as realistic as possible, we gave these models a realistic thickness of 92 to 100 Å. We also built two models for the diffraction simulations, which we made 460 Å thick.

3. Microdiffraction along dislocation cores

We propose the measurement of the core period using a sub-nanometre STEM probe with the beam aligned along the partial dislocation core as illustrated in figure 2. We treat the simple case of the 90° partial in Si, for which doubling of the core period due to a novel (and controversial) reconstruction has recently been suggested [7]; however our method is general. In this case the stacking sequence for the perfect crystal is ABAB... along [110], and all core displacements lie in these (110) planes, normal to the beam, except those related to the dimerization or period doubling along the core. This line defect will give rise to a sheet of diffuse scattering at half the height of the first-order Laue zone (FOLZ) of reflections from the perfect crystal, as shown in figure 1. The Ewald sphere intersects this sheet in a circle, which

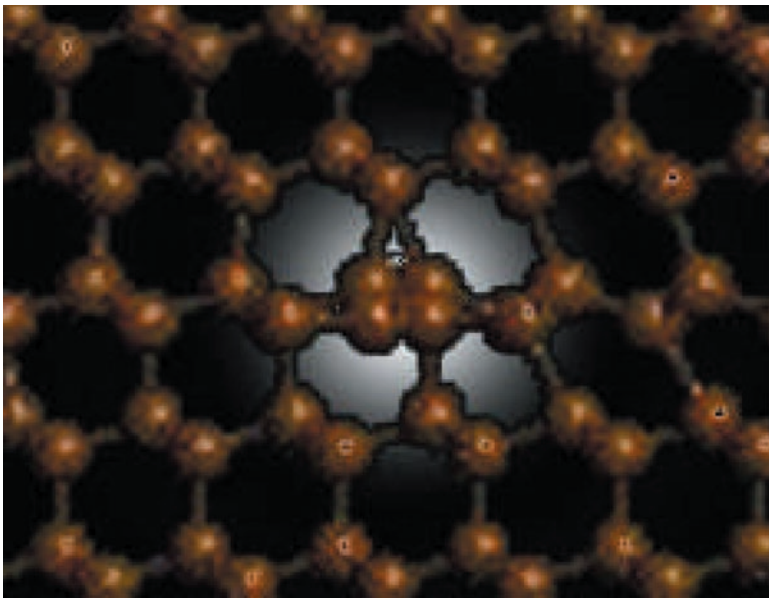

Figure 2. Diagram of position and size of the CBED probe with respect to the dislocation core shown here for the case of the DP reconstructed core of the 90° partial in Si in the (−110) projection.

will appear in the CBED pattern as shown at a radial distance

$$\frac{A}{B} = \frac{1}{2}\sqrt{\frac{2-\lambda/2a}{1-\lambda/2a}} \simeq \frac{1}{\sqrt{2}}$$

times that of the FOLZ where λ is the incident electron beam wavelength and a the length of the unit cell (of the perfect crystal) along the beam direction. For high energies, i.e. $\lambda \ll a$, we have $A/B = 1/\sqrt{2}$.

Using the structural models for the double period reconstruction (DP) given by Bennetto *et al* [7] and the single period model [6], we have performed multislice calculations, using an 8 nm×8.5 nm supercell. The sample thickness is 46 nm. The convergent electron probe wavefunction is placed in the first slice of the multislice, centred over the dislocation core. The probe is synthesized by Fourier transformation of the function $A(u)\chi(u)$, where $A(u)$ is a top-hat objective aperture function for the STEM and $\chi(u)$ is the usual aberration function for the probe-forming lens [8]. Figure 2 shows the size of the probe relative to the lattice. The probe is stationary and we record the entire microdiffraction pattern. Using an aperture size of 4 mrad, $C_s = 0.7$ mm, and defocus settings $d_f = 509$ Å and $u_0 = \Theta/\lambda = 0.16$ Å^{-1} [8], the probe width is approximately $w = 1$ nm as expected.

The resulting patterns shown in figure 3 for 100 keV electrons show a broadened ring of diffuse scattering at the expected position for the DP model. Experimentally, energy filtering of only the elastically scattered electrons can be expected to greatly reduce background, while a field-emission source will increase intensity. The ring is broadened by the incident beam divergence. This method has the advantage over HREM methods that a high probe intensity is concentrated just on the atoms of interest. Compared to HREM imaging from the side, a larger number of atoms contribute to the wanted signal. The radius of the ring gives the core period. For perfect crystals it is readily shown that the intensity distribution in these patterns

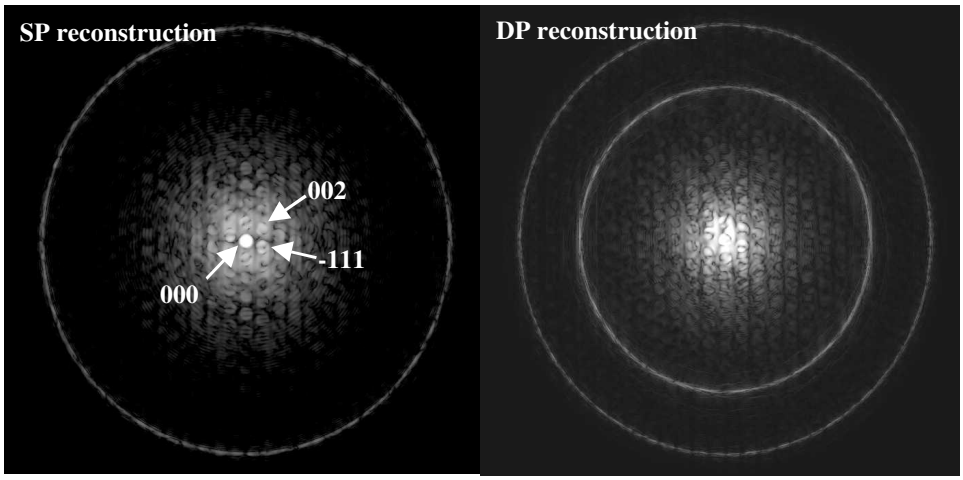

Figure 3. Computed dynamical microdiffraction patterns with STEM probe stationary along core of 90° partial dislocation in Si. The additional ring at $1/\sqrt{2}$, the radius of the FOLZ ring, clearly distinguishes the DP from the SP reconstruction. The intensity is displayed on a logarithmic scale.

does not depend on focus setting if the diffraction discs do not overlap [16]. Since diffuse elastic scattering due to the non-periodicity of the core structure in the directions perpendicular to the beam is present, these patterns do depend on the focus setting; however the position of the ring is insensitive to this.

4. Imaging kinks by HREM

Striking bright-field TEM images of the surfaces of ceramics have recently been obtained [4, 9] using a high temperature anneal process which results in atomically smooth terraced surfaces which are preserved at atmospheric pressure. Our kink imaging method [3] is limited by surface roughness. We are therefore attempting to apply it to samples of cubic (β-) SiC. This material has almost the same structure (zinc-blende instead of diamond cubic) and therefore the same needed forbidden reflections, which oscillate with about twice the amplitude (hence four times the intensity) of the forbidden reflections in Si and should therefore give even stronger imaging contrast.

In order to show the improvement in image quality we would get from atomically flat surfaces we simulated the effects of surface roughness for our Si models. We randomly distributed a number of atoms across the surface and added more atoms to it, which would 'move around' in a random walk manner until they found neighbours to settle next to and thereby form small atomic clusters on the surface. These islands were up to 3 Å thick, i.e. just thick enough to produce forbidden reflections. The simulated images using the FRLI method showed the same washing out of details along the stacking fault boundary as the experiment [3], which raises our expectations to get much better results with SiC.

Figure 4 shows a Pendellösung plot for the amplitude of the $(-422)/3$ Bragg reflection as a function of thickness in SiC for a [111] beam direction. This amplitude is zero for slabs containing $3n$ double layers and also for the second order $2/3(-422)$ forbidden reflection. A stacking fault (SF) has been included. We see that the amplitude of these beams when diffracted from a region containing a SF is higher than the amplitude of a corresponding beam passing through faultless material for two out of three possible terminations (either B, or C

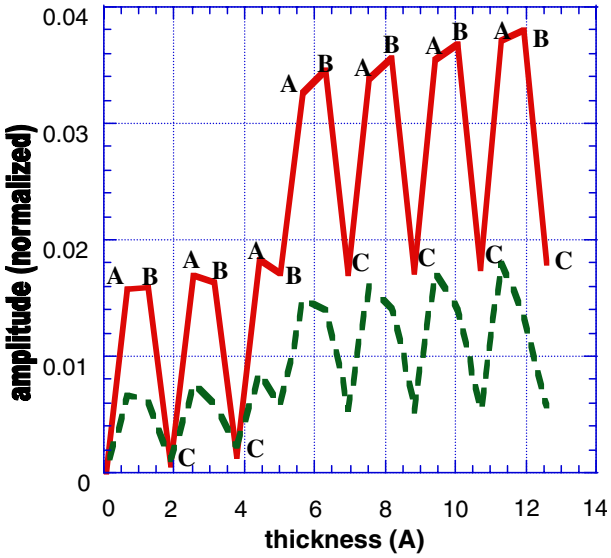

Figure 4. Pendellösung plot of the dynamical 1/3(−422) (solid) and 2/3(−422) (dashed) Bragg reflections in SiC including an intrinsic stacking fault (FCC layer stacking sequence ABCABC... for (111) orientation). For a perfect crystal the intensity is zero after $3n$ layers. Once the electron beam passes through the stacking fault, its intensity stays non-zero.

as the last layer in the faultless region). This large difference in amplitude may be used to form lattice images from these reflections. The SF may also be imaged using dark field on the (−422)/3 type reflections.

Samples of β-SiC film on Si(111) have been indented at 800 and 1000 °C in air at a loading of 50 g for 5 s using a Vickers indenter apparatus. Thin slabs with [111] normals are prepared by ultrasonic cutting, and wedge-polishing in order to obtain images of SF in this geometry. The boundaries of the SF ribbon delineate the dislocation cores, and may reveal any kinks, impurities, solitons and other defects on them.

5. New application of spherical aberration corrected TEM

The development of several ultra-high resolution schemes (see [10] for a summary of seven new approaches) including the use of aberration correctors, high voltage microscopes and through-focus schemes, promise that a resolution of about one ångström will be routinely available for HREM in the near future (site permitting). This raises the question of whether one might be able to distinguish kink models from this type of image, viewed normal to the dislocation line, using forbidden reflections. Earlier simulations for kink images at 0.3 nm resolution [11] were unable to do this.

Since forbidden reflections in Si as well as SiC are very weak compared to the bulk reflections, the only way to obtain high image contrast from the stacking fault is to allow only the forbidden reflections to contribute to the image and block the bulk reflections by an appropriate objective aperture. If we wanted to record images at a higher resolution with similar image contrast we would therefore need a ring aperture that blocks the bulk reflections, but lets higher order forbidden reflections pass. Such an aperture is very difficult to realize mechanically, but if we take a closer look at the microscope transfer function (MTF), we see

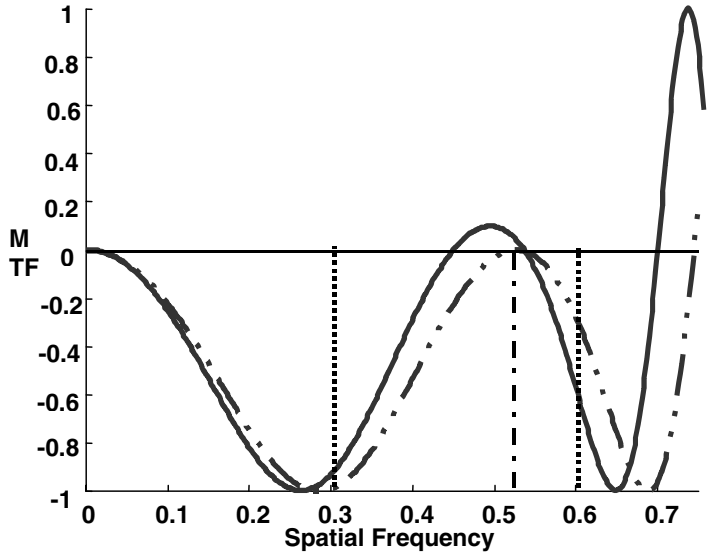

Figure 5. MTF for 200 keV, $C_s = 0.1652$ mm, $d_f = 288$ Å (dashed), which gives $\sin(\chi(k_B)) = 0$ for Si, and $C_s = 0.225$ mm, $d_f = 341$ Å (solid), the optimized MTF using equation (1). The vertical lines indicate the position of the first and second order forbidden reflections (solid) and the bulk reflection (dashed) for Si.

that we can use the objective lens as a tunable ring aperture, if we are able to adjust the spherical aberration. Recently the first spherical aberration (C_S) corrected TEM has been demonstrated [12].

The electron wavefunction Ψ_0 is convoluted with the objective lens transfer function giving the wavefunction in the image plane (Ψ_i) according to [5]

$$\Psi_i(x) = \Psi_0(x) \otimes \mathrm{FT}[\exp(-\mathrm{i}\chi(k))A(k)] \tag{1}$$

$$|\Psi_i(x)|^2 \cong 1 + 2\mathrm{FT}[\varphi(k)\sin(\chi(k))] \tag{2}$$

$$\chi(k) = \tfrac{1}{2}\pi\lambda^3 C_s k^4 - \pi\lambda d_f k^2 + \cdots. \tag{3}$$

Here λ is the electron wavelength, k the coordinate in reciprocal space ($k = 1/x$), Ψ_0 is the wavefunction at the exit face of the crystal, d_f is the defocus and $A(k)$ is a top-hat function describing the objective aperture. $\Psi(k)$ is the Fourier transform of $\Psi(x)$. Equation (2) assumes that $\Psi_0(x)$ can be expanded as $1 + \mathrm{i}\varphi(x) + \mathrm{O}(\varphi(x)^2)$. There are a lot more terms in (3), but we will restrict ourselves to the most dominant ones for illustrative reasons. According to equations (2) and (3) one can find a combination of C_S and d_f analytically for any given λ which lets $\sin(\chi(k))$ go to zero for the lowest bulk allowed spatial frequency k_B but 1 or -1 for the lowest order forbidden reflection k_F and again non-zero for the second order forbidden reflection at $2k_F$. Figure 5 shows such a MTF ($\sin[\chi(k)]$) as the dash–dotted curve.

Since (2) is only valid for weak phase objects unlike our 10 nm thick samples, we optimized the parameters C_S and d_f with respect to the ratio of I_F/I_B, the ratio of intensities of the spatial frequency components k_F and k_B in the image $|\Psi_i|^2$ for our more realistic fully dynamical Ψ_0 that we obtained from the multislice calculations using (1). For a 200 keV TEM with $C_S = 0.225$ mm and $d_f = 341$ Å this ratio becomes 1.2×10^4, which means that the contribution of the first and second order forbidden reflections is much stronger than the

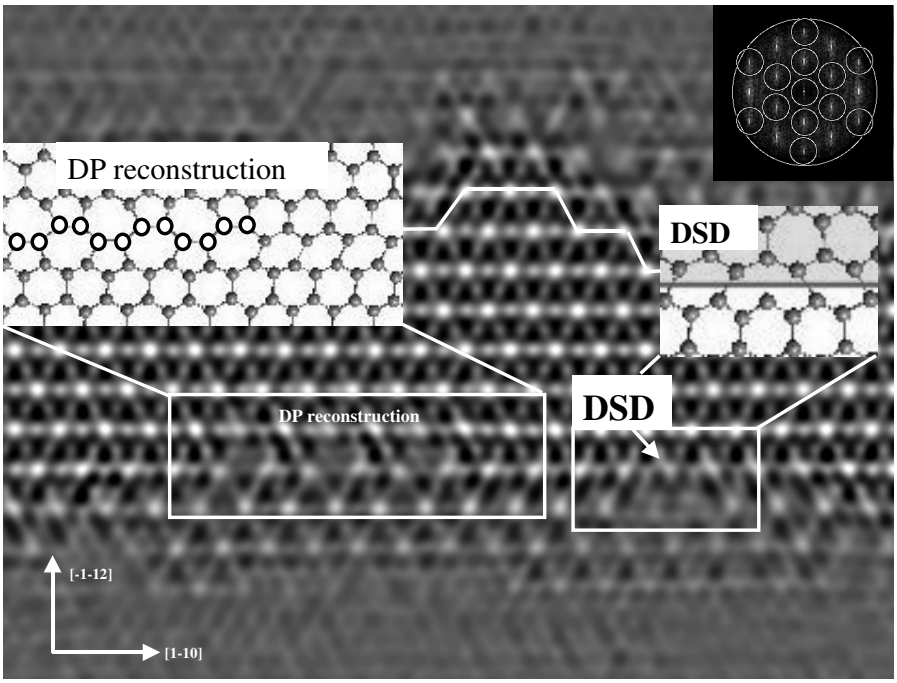

Figure 6. HREM image simulation for a 90° partial dislocation dipole in which each partial contains several defects including kinks and direction switching defects (DSD). Crystallographic directions are indicated in the figure. The thickness is 10 nm and resolution is limited to 0.15 nm. The white line indicates a combination of different kink structures. The phase switching defect as well as the core region with DP structure can easily be seen in this simulation.

contribution of the bulk reflections. This will allow us to record an image with an objective aperture about twice as large as the one used for the conventional FRLI method [3]. The corresponding MTF is shown in figure 5 as the solid curve. It should be noted here that the increase in objective aperture size means an increase in resolution by a factor of two, but with restrictions. Since the stacking fault also produces bulklike reflections, we will be filtering away some periodic information from the stacking fault image as well as part of the diffuse scattering due to non-periodic features like the stacking fault boundary. However, this method still means a considerable increase in resolution in comparison with the conventional FRLI method.

In order to eliminate any residual bulk contribution to the image we subtracted the image of an unfaulted crystal from the one containing the SF. This can easily be realized in the experiment by making sure that the exposure contains a region of perfect crystal, which can then be subtracted from the region containing the SF. In addition to this subtraction we also applied a Fourier filtering technique. Figure 6 shows the multislice simulation for samples with atomically smooth surfaces and kinks on the 90° partial running along [−110] in Si, viewed along [111] with the (111) SF in the middle of a (111) slab of Si 10 nm thick. A TEM similar to the one used by Haider *et al* [12] is assumed at 200 keV. The resolution is limited to 0.15 nm by an objective aperture transmitting beams up to $k\lambda = \alpha_{max} = 17$ mrad. The inset in figure 6 shows the *a posteriori* spatial filtering of this image that has been applied in order to remove all the bulk allowed reflections from the image. Only the spatial frequencies contained within the white circles are present in the image.

We see that the position of the kink can be clearly identified to within an accuracy of less than 0.3 nm. This resolution improvement, combined with the surface smoothing effect of an anneal will make accurate measurements of the kink density possible, and will also allow the identification of obstacles along the line. A measurement of the density of these would allow one to distinguish between the theory of Hirth and Lothe [13] of dislocation motion (as limited by kink formation or migration energies) and the theory of Celli *et al* [14], in which obstacles provide the rate-limiting step.

Apart from the exact outline of the SF, different kinds of defect can be detected, such as direction switching defects along the SP reconstructed 90° partial and also whether we have SP or DP reconstruction. The simulations for the 30° partial (not shown here) even show some differences between different kink models proposed by [6].

6. Conclusion

We have proposed a new method to detect whether the core along the 90° partial is double period reconstructed, which does not require any special equipment or a particular way of sample preparation. The result will be interpretable without ambiguity.

We have also shown how we can increase the quality of stacking fault boundary images, by using materials that have inert atomically flat surfaces after a special annealing procedure. Atomically flat surfaces will then also make imaging at higher resolution possible, which we propose can be done using an optimized combination of spherical aberration and defocus in an aberration corrected transmission electron microscope.

This increase in resolution shows differences between different kink structures in the simulation, which might finally be detected using HRTEM imaging. However, the simulations were done for perfect conditions, and we will have to confirm them with experimental results, which will be reported in a later paper, before drawing further conclusions. However, it might open the possibility of finding new kink structures by comparing experimental images with image simulations like the ones shown here.

Acknowledgments

The first author would like to thank C Zorman and M Mehregany from Case Western Reserve University for providing the samples and also Professor P Pirouz and J Chung from CWRU for producing the indents in them.

This work was supported by NSF award DMR9814055.

References

[1] Chelikowski J and Spence J C H 1984 *Phys. Rev.* B **30** 694
[2] Jones R 2000 *Mater. Sci. Eng.* B **71** 24
[3] Kolar H, Spence J C H and Alexander H 1996 *Phys. Rev. Lett.* **77** 4031
[4] Suznitsky D and Carter C 1991 *J. Mater. Res.* **6** 2403
[5] Kirkland E J 1998 *Advanced Computing in Electron Microscopy* (New York: Plenum)
[6] Nunes R W, Benetto J and Vanderbilt D 1998 *Phys. Rev.* B **57** 10 388
[7] Bennetto J, Nunes R and Vanderbilt D 1997 *Phys. Rev. Lett.* **79** 245
[8] Spence J C H and Zuo J M 1992 *Electron Microdiffraction* (New York: Plenum)
[9] Ndbubuisi G, Liu J and Cowley J M 1992 *Microsc. Res. Tech.* **21** 10
[10] Spence J C H 1999 *Mater. Sci. Eng.* R **26** 1
[11] Spence J C H 1981 *Proc. 39th EMSA Meeting (Claitors)* ed G Bailey, p 120
[12] Haider M *et al* 1998 *Ultramicroscopy* **75** 53–60

[13] Hirth J P and Lothe J 1982 *Theory of Dislocations* (New York: Wiley)
[14] Celli V, Kabler M, Nimomiya T and Thomson R 1963 *Phys. Rev.* **131** 58
[15] Cherns D 1974 *Phil. Mag.* **30** 549
[16] Spence J C H and Cowley J M 1978 *Optik* **50** 129